Version of accepted author manuscript; published in final form in
Organic Geochemistry, 65, 53-62 doi: 10.1016/j.orggeochem.2013.09.012

Comprehensive glycerol ether lipid fingerprints through a novel reverse-phase liquid chromatography-mass spectrometry protocol

Chun Zhu*, Julius S. Lipp, Lars Wörmer, Kevin W. Becker, Jan Schröder, Kai-Uwe Hinrichs

Organic Geochemistry Group, MARUM Center for Marine Environmental Sciences and Dept. of Geosciences, University of Bremen, P.O. Box 330 440, 28334 Bremen, Germany

*To whom correspondence should be addressed. E-mail: czhu@uni-bremen.de

Version of accepted author manuscript; published in final form in
Organic Geochemistry, 65, 53-62 doi: 10.1016/j.orggeochem.2013.09.012

Abstract

Glycerol ether lipids have been developed as proxies to reconstruct past environmental changes or in their intact polar form to fingerprint the viable microbial community composition. However, due to the structural complexity, the full characterization of glycerol ether lipids requires separate protocols for the analysis of the polar head groups and the alkyl chain moieties in core ether lipids. As a consequence, the valuable relationship between core ether lipid composition and specific polar head groups is often lost; this limits our understanding of the diversity of ether lipids and their utilities as biogeochemical proxies. Here, we report a novel reverse-phase liquid chromatography-electrospray ionization-mass spectrometry (RP-ESI-MS) protocol that enables the simultaneous analysis of polar head groups (e.g., phosphocholine, phosphoglycerol, phosphoinositol, hexose, and dihexose) and alkyl moieties (e.g., alkyl moieties modified with different numbers of cycloalkyl moieties, hydroxyl and alkyl groups, and double bonds) in crude lipid extracts without further preparation. This protocol greatly enhances the detection of archaeal intact polar lipids (IPLs) and core lipids (CLs) with double-bond-and hydroxyl-group-bearing alkyl moieties. With these improvements, widely used ratios that describe relative distribution of the core lipid, such as the TEX_{86} and ring index, can now be directly determined in specific intact polar lipids (IPL-specific TEX_{86} and ring index). Since IPLs are the putative precursors of the environmentally persistent core lipids, their detailed examination by this protocol can potentially provide new insights into diagenetic and biological mechanisms inherent to these proxies. In a series of 12 samples from diverse settings, core and IPL-specific TEX_{86} values follow the order: 2G-GDGTs > core GDGTs > 1G-GDGTs > 1G-GDGT-PI; and the ring indices follow: 1G-GDGTs ≈ core GDGTs > 2G-GDGTs > 1G-GDGT-

Version of accepted author manuscript; published in final form in
Organic Geochemistry, 65, 53-62 doi: 10.1016/j.orggeochem.2013.09.012

P1G > 2G-OH-GDGTs ≈ 1G-OH-GDGTs (abbreviations: 1G = monoglycosyl; 2G = diglycosyl; OH = hydroxyl; P1G = phospho-monoglycosyl; GDGT = glycerol dialkyl glycerol tetraether).

Key words: intact polar lipids (IPLs), GDGTs, reverse-phase, TEX_{86}, OH-GDGTs, LC-MS

Version of accepted author manuscript; published in final form in
Organic Geochemistry, 65, 53-62 doi: 10.1016/j.orggeochem.2013.09.012

1. Introduction

Valuable taxonomic and environmental information is encoded in membrane-derived glycerol ether lipids found in all Archaea and some Bacteria. These lipids mainly consist of glycerol dialkyl glycerol tetraethers (GDGTs) and dialkyl glycerol diethers (DGDs), both of which are found in environmental samples as intact polar lipids (IPLs) associated with polar head groups, and core lipids (CLs) without head groups (Fig. 1). Since the head groups, particularly those based on phosphate esters, are cleaved from the ether core lipids quickly after cell death (White et al., 1979; Harvey et al., 1986), IPL distributions serve as microbial fingerprints that reveal information on the *in situ* viable community composition in marine subsurface sediments and water columns (Biddle et al., 2006; Lipp et al., 2008; Schubotz et al., 2009). By contrast, CLs are relatively recalcitrant and can persist over geological time scales in marine sediments (Bolle et al., 2000; Kuypers et al., 2001). Lipid proxies take advantage of the fact that many microorganisms adjust their lipid composition in response to environmental changes (e.g., Gibson et al., 2005; Weijers et al., 2007; Wuchter et al., 2004). Consequently CLs preserved in marine sediments are being used to develop proxy records, e.g., the TEX_{86} (Schouten et al., 2002) and CBT/MBT proxies (Weijers et al., 2007), from which past environmental changes are inferred.

Given the significance of glycerol ether lipids, several analytical methods have been progressively developed. Gas chromatography-mass spectrometry (GC-MS)was used for analysis of DGDs such as archaeol (AR; Fig. 1) and hydroxy-archaeol (OH-AR; Fig. 1) (e.g., Hinrichs et al., 1999; Elvert et al., 2003). The analytical window was extended to include liquid chromatography-mass spectrometry (LC-MS) methods. The established approach is based on normal-phase liquid chromatography-atmospheric pressure chemical ionization-MS (NP-APCI-

MS (Hopmans et al., 2000; Schouten et al., 2007); which separates GDGTs according to different rings or methyl groups on the alkyl moieties and resulted in the establishment of protocols for determination of the TEX_{86} (Schouten et al., 2002) and CBT/MBT proxies (Weijers et al., 2007). However, there are drawbacks using GC-MS and NP-APCI-MS for glycerol ether lipid analysis. First, both techniques are suitable for analysis CLs but cannot directly analyze IPLs without prior head group cleavage. Moreover, APCI causes in-source degradation of ether lipids at varying degree, depending on the CL structures. For example, conventional GDGTs are subjected to minor in-source fragmentation (Byrdwell, 2001; Huguet et al., 2006)whereas hydroxylated GDGTs (OH-GDGTs; Fig. 1) lose the tertiary hydroxyl group, and consequently yield artificial unsaturated GDGTs as base peaks identical to protonated ring-bearing GDGTs (Liu et al., 2012), in analogy to hydroxylated fatty acids (Ikeda and Kusaka; 1992 Byrdwell, 2001).

IPLs have largely been analyzed by normal-phase liquid chromatography-electrospray ionization-multiple stage mass spectrometry (NP-ESI-MS) (e.g., Rütters et al., 2001; Sturt et al., 2004; Zink and Mangelsdorf, 2004). With NP-ESI-MS, IPLs are chromatographically separated according to head group polarity, while lipids with identical head groups tend to largely co-elute, despite considerable structural diversity of the respective core moieties. CLs are not chromatographically retained using common analytical protocols for IPL analysis due to their low polarity. Therefore, valuable information from the ether cores remains inaccessible.

Since none of the above mentioned protocols can fully characterize a sample's inventory of ether lipids, additional sample preparation is employed and typically includes separation of the total lipid extract into a polar (IPL-containing) and an apolar (core lipid-containing) fraction followed by acid hydrolysis of the polar fraction to cleave off head groups (Knappy et al., 2009;

Lipp and Hinrichs, 2009; Huguet et al., 2010; Liu et al., 2011; Pitcher et al., 2011). The polar fraction is analyzed by NP-ESI-MS for IPLs and subsequently analyzed again by NP-APCI-MS after acid hydrolysis for hydrolysis-derived core lipids. However, there are several shortcomings: 1) the relationship between specific core moieties and specific head groups is lost; 2) hydrolysis of the polar fraction could generate core lipids from diagenetically formed polar precursors; 3) byproducts may be formed from hydroxylated lipids during the acid hydrolysis (Koga and Morii, 2005); 4) sample preparation is labor-intensive and time-consuming.

Reverse-phase (RP) chromatography coupled to either APCI- or ESI-MS has been employed to analyze crude lipid mixtures or lipid classes (Byrdwell, 2001; Nichols and Davies, 2002; Willmann et al., 2011). RP chromatography can separate fatty acids according to acyl chain length and degree of unsaturation (e.g., Aveldano et al., 1983; Larsen et al., 2002; Sommer et al., 2006). Recently, Wörmer et al. (2013) developed a RP-ESI-MS method that takes advantage of new chromatographic technologies such as smaller particle size (1.7µm) and new column fillings; the resulting method improves detection limits for IPL analysis but does not achieve the chromatographic resolution for full characterization of the core moieties of bacterial and archaeal ether lipids.

In order to address these limitations in lipid fingerprinting, we developed an improved RP-ESI-MS protocol that simultaneously elucidates structures of both head groups and core moieties of ether lipids without sample preparation and report for the first time directly determined IPL-specific TEX_{86} values and ring indices. This RP-ESI-MS protocol resulted in greatly improved detection of IPLs and labile core ether lipids that previously escaped detection due to unsuitable ionization with APCI. The new method therefore yields novel and comprehensive information on lipid fingerprints.

Version of accepted author manuscript; published in final form in
Organic Geochemistry, 65, 53-62 doi: 10.1016/j.orggeochem.2013.09.012

2. Materials and methods

2.1. Materials

2.1.1. Samples

Samples were collected from diverse depositional settings including the Mediterranean Sea, the Black Sea, the Sea of Marmara, the Peruvian margin, and a cold seep off Pakistan (Table 1). The Black Sea represents atypical euxinic marine basin connected to the well ventilated, oligotrophic Mediterranean Sea through the Sea of Marmara. The Peru margin is characterized by high surface-ocean productivity and its sediments are organic-rich silts. The cold seep site is located at the convergent continental margin off Pakistan where focused upward migration of methane stimulates high rates of anaerobic oxidation of methane (AOM) (Fischer et al., 2012).

2.1.2. Standards and reagents

Ether lipid standards of ß-L-gulosyl-phosphoglyceroldibiphytanyl glycerol tetraether (Gul-GDGT-PG) and phosphoethanolamine-archaeol (PE-AR) were purchased from Matreya, LLC, Pleasant Gap, PA, USA, and Avanti Polar Lipids Inc., USA, respectively. $GDGT_0$ (Fig. 1) was isolated and purified from a culture of *Archaeoglobus fulgidus*. These lipids were used as IPL and CL representatives to optimize the ESI-MS conditions. LC-MS grade methanol was obtained from Merck Chemicals (Darmstadt, Germany). LC-MS grade hexane, 2-propanol, and solutions of formic acid (98%) and NH_4OH (>25% NH_3) were purchased from Sigma Aldrich (Steinheim, Germany).

2.1.3. Columns

Version of accepted author manuscript; published in final form in
Organic Geochemistry, 65, 53-62 doi: 10.1016/j.orggeochem.2013.09.012

An analytical ACE3 C_{18} column (3 µm, 2.1 × 150 mm) was purchased from Advanced Chromatography Technologies Ltd., Aberdeen, Scotland for simultaneous RP analysis of CLs and IPLs. Analytical Grace LiChrospher Diol (5 µm, 2.1 × 150 mm) and Prevail Cyano (CN; 3 µm, 2.1 ×150 mm) columns were purchased from Alltech Associates Inc., Deerfield, IL, USA, for normal-phase analysis of IPLs and CLs, respectively. Lipid purification was based on a set of orthogonal semi-preparative columns: an Inertsil Diol column (5 µm, 150 × 10 mm, GL Sciences Inc., Tokyo, Japan) for NP preparation, and a Zorbax Eclipse XDB-C_{18} column (5 µm, 250 × 9.4 mm, Agilent Technologies Deutschland GmbH, Böblingen, Germany) for RP separation.

2.2. Sample preparation

Samples were freeze-dried and extracted using a modified Bligh and Dyer method (Sturt et al., 2004). The obtained total lipid extracts (TLEs) were split into three aliquots for RP-ESI-MS, NP-ESI-MS, and apolar-polar separation, respectively. The apolar-polar separation was achieved using a silica gel column (Oba et al., 2006) and the resulting polar fraction was hydrolyzed (Lipp and Hinrichs., 2009). The apolar and hydrolyzed polar fractions were analyzed using NP-APCI-MS.

2.3. Instrumentation

2.3.1. RP- and NP-ESI-MS$_{qTOF}$

RP-ESI-MS and NP-ESI-MS analyses were performed on a Dionex Ultimate 3000 UHPLC coupled to a Bruker maXis Ultra High Resolution orthogonal acceleration quadrupole－time-of-flight (qTOF) tandem MS/MS, equipped with an ESI source and operated in positive ion mode (Bruker Daltonik, Bremen, Germany). RP and NP chromatographic separation of ether lipid

mixtures was achieved on a C_{18} and Diol column (Section 2.1.3. Columns), respectively, and details are provided in Table 2. The optimized ESI-$MS_{(qTOF)}$ settings for $RP_{(C18)}$ chromatography were: capillary voltage 4500 V, nebulizing gas pressure 0.8 bar, and dry gas 4 L/min at a temperature of 200°C, in source collision-induced energy (ISCID) 0 eV. And the ESI-$MS_{(qTOF)}$ settings for $NP_{(Diol)}$ chromatography were: capillary voltage 4500 V, nebulizing gas pressure 2.0 bar, and dry gas 6 L min^{-1} with a temperature of 200°C. Other parameters (e.g. ion transfer, collision, and detection) were identical to the $RP_{(C18)}$-ESI-MS $method_{(qTOF)}$.

For both $RP_{(C18)}$- and $NP_{(Diol)}$-ESI-$MS_{(qTOF)}$ methods, the scanned range was from *m/z* 100 to 2000 in positive ion mode at a scan rate of 1 Hz with automated data-dependent fragmentation of the three most abundant ions. Mass accuracy was monitored by both a tuning mixture solution (*m/z* 322.0481, 622.0290, 922.0098, 1221.9906, 1521.9715, and 1821.9523) introduced by loop-injection near the end of a run and an internal lock mass (hexakis-(1H,1H,3H-tetrafluoro-pentoxy)phosphazene, *m/z* 922.0098) throughout the entire run. Lipids were identified by retention time, accurate masses (typically better than1 ppm mass accuracy),and diagnostic fragments based on Sturt et al. (2004) and Yoshinaga et al. (2011). The LC-MS data were processed through Data Analysis 4.0 software (Bruker Daltonik, Bremen, Germany). Protonated $[M+H]^+$, ammoniated $[M+NH_4]^+$, and sodiated $[M+Na]^+$ pseudo molecular ions are common for non-amide containing lipids and were thus included for quantification. PC- and PE-containing lipids are quantified by $[M]^+$ and $[M+H]^+$, respectively. If doubly charged ions such as $[M+NH_4+NH_4]^{2+}$, $[M+H+H]^{2+}$, and $[M+NH_4+Na]^{2+}$ occur, they were also included in the integration. The extraction window of individual ion chromatograms is ± 0.05*m/z* units.

2.3.2. NP-APCI-MS_{MSD}

177 The conventional NP-APCI-MS analysis of core GDGTs was based on Schouten et al. (2007)
178 and implemented on an Agilent 1200 series HPLC coupled to an Agilent 6130 MSD via a
179 multimode interface (MMI) set to APCI mode (Agilent Technologies, Waldbronn, Germany),
180 Chromatographic separation of core GDGTs was achieved on a CN column with details shown
181 in Table 2. The APCI-$MS_{(MSD)}$ conditions were optimized according to Liu et al. (2012). Both a
182 full scan (*m/z* 500-1500; 50% of cycle time) and selected ion monitoring (SIM; 50% of cycle
183 time) for individual GDGTs were recorded. Lipids were scanned by $[M+H]^+ \pm 0.5 m/z$ units
184 whereas OH-GDGTs are scanned by $[M+H-H_2O]^+ \pm 0.5$ *m/z* due to in-source dehydration (cf.
185 Liu et al., 2012).
186
187 *2.3.3. Impact of ionization mode*
188 The impact of ionization mode, i.e., APCI vs. ESI, on the detection of unsaturated and
189 hydroxylated ether lipids was evaluated by changing the MMI mode from $NP_{(CN)}$-$APCI\text{-}MS_{(MSD)}$
190 to $NP_{(CN)}$-$ESI\text{-}MS_{(MSD)}$ while keeping the fragmentor voltage and LC conditions constant, with
191 post column buffer addition (100:0.12:0.04 of 2-propanol/formic acid/14.8 M NH_3) via T-piece
192 to assist electrospray ionization.
193
194 *2.3.4. Detection limits*
195 In order to compare the detection limit for core GDGTs between the new $RP_{(C18)}$-ESI-MS
196 and conventional $NP_{(CN)}$-APCI-MS protocols, a dilution series (sample # 1; Table 1) was
197 analyzed by the two methods, respectively, on the Dionex Ultimate 3000 UHPLC/qTOF under
198 respective optimum conditions (i.e., $RP_{(C18)}$-$ESI\text{-}MS_{(qTOF)}$ vs. $NP_{(CN)}$-$APCI\text{-}MS_{(qTOF)}$). Core
199 GDGTs were detected by scanning from *m/z* 500-2000 in positive (ESI+ and APCI+) ion mode.

200

201 *2.3.5. Mono and diglycosidic GDGT isolation*

202 Mono- and diglycosidic (1G, 2G) GDGTs (Fig. 1) were isolated from TLE of a sediment
203 sample (sample # 13; Table 1) through orthogonal columns on an Agilent 1200 series HPLC
204 equipped with an Agilent 1200 series fraction collector. In brief, TLE was dissolved in hexane:
205 2-propanol (7:3, v/v) and separated first by a semi-preparative Inertsil Diol column maintained at
206 30°C. IPLs were eluted by linear gradient from 100% A to 90% A: 10% B in 5 min, and
207 subsequently to 40% A: 60% B in another 18 min, where A is hexane:2-propanol (85:15, v/v)
208 and B is 2-propanol:water (90:10, v/v) at a flow rate of 3 mL min^{-1}. The column was cleaned by
209 15% A: 85% B for 7 min and re-equilibrated with 100% A for another 10 min. Fractions
210 containing 1G- and 2G-GDGT were collected in the time windows of 5.1-8.7 min and 11.7-15.4
211 min, respectively, and subjected to a second step of reverse-phase purification through a semi-
212 preparative Zorbax Eclipse XDB-C_{18} column operated at 45°C. Samples were re-dissolved in
213 methanol:2-propanol (8:2, v/v) and eluted by linear gradient from 80% methanol: 20% 2-
214 propanol to 60% methanol: 40% 2-propanolin 5 min, and then to 35% methanol: 65% 2-propanol
215 in another 40 min with a flow rate of 2.2 mL min^{-1}. The column was washed by 100% 2-
216 propanol for 15 min followed by column re-conditioning with 100% methanol for another 15
217 min. 2G- and 1G-GDGTs were collected in the time windows of 35.5 - 43.5 min and 43.5 – 50
218 min, respectively.

219

220 **2.3. Validation of IPL-specific TEX_{86}determination**

221 An aliquot of each of the purified 1G- and 2G-GDGT fraction was directly analyzed by
222 $RP_{(C18)}$-ESI-$MS_{(qTOF)}$ to obtain 1G- and 2G-GDGT-specific TEX_{86} values. Another aliquot was

Version of accepted author manuscript; published in final form in
Organic Geochemistry, 65, 53-62 doi: 10.1016/j.orggeochem.2013.09.012

hydrolyzed to cleave off the head groups using the method by Lipp and Hinrichs (2009), and subsequently analyzed by $NP_{(CN)}$-APCI-$MS_{(MSD)}$, respectively. TEX_{86} values and ring indices of both core GDGTs and specific IPL-GDGTs were calculated according to Schouten et al. (2002) and Pearson et al. (2004), respectively.

3. Results and discussion

3.1. Improved chromatography and detection of archaeal IPLs

Figs. 2 and 3 illustrate the detection of intact di- and tetraether lipids using the $RP_{(C18)}$-ESI-$MS_{(qTOF)}$ and $NP_{(Diol)}$-ESI-$MS_{(qTOF)}$ method, respectively. For all tested samples, the former method displays much sharper peaks, higher sensitivity, and higher signal to noise (S/N) ratios for ether lipids than the latter method. In particular, monoglycosyl ether lipids, for example 1G-GDGTs, commonly have broad peaks with short retention times close to the injection peak after NP analysis. Consequently, 1G-GDGT signals are generally weak or even non-detectable in most environmental samples (Fig. 3B). Reduction of the polarity of eluent A from original 79:20:0.12:0.04 (Sturt et al., 2004) to 85:15:0.12:0.04 (hexane/2-propanol/formic acid/14.8 M NH_{3aq}) in the $NP_{(Diol)}$-ESI-$MS_{(qTOF)}$ protocol did not improve chromatography but resulted in precipitation of salts. This weakness is overcome by RP analysis, where such lipids are excellently retained and separated as reflected by a series of sharp, well separated peaks of 1G-GDGTs (Fig. 3A). This clearly suggests that the applied RP protocol greatly improves the chromatography of archaeal IPLs and thus results in strongly enhanced archaeal IPL detection on $RP_{(C18)}$ relative to $NP_{(Diol)}$, consistent with analogous observations for ester-bound, bacterial-type IPLs using the RP protocol by Wörmer et al. (2013).

The most important advantage of the RP protocol introduced here is the ability to separate both IPLs and CLs according to subtle structural variations on the alkyl chains such as different numbers of cycloalkyl moieties (Figs. 3A and 4A) and different degrees of methylation (Fig. 4B), hydroxylation (Fig. 4C), and unsaturation (Fig. 4C). Notably, the high chromatographic resolution of GDGTs with varying numbers of cycloalkyl moieties leads to direct determination of TEX_{86} values and ring indices for not only core GDGTs (core-TEX_{86} and ring indices), but also, for the first time, specific GDGT IPLs (IPL-specific TEX_{86} and ring indices), providing an important basis to study biological and diagenetic mechanisms of empirically established proxies.

3.2. Fidelity of RP-ESI-MS for proxy determination

Core lipids and related proxies are commonly quantified by the conventional $NP_{(CN)}$-APCI-MS; the $RP_{(C18)}$-ESI-MS protocol introduced here utilizes ESI as ionization mode. Therefore, it is necessary to compare the detection limit of GDGTs and the quantification of TEX_{86} proxy between the two ionization modes.

A dilution series of core GDGTs display comparable detection limits for $NP_{(CN)}$-APCI-$MS_{(qTOF)}$ and $RP_{(C18)}$-ESI-$MS_{(qTOF)}$ on the same instrument with respective optimum conditions (~10 pg on column with S/N > 5). The core- and IPL-specificTEX_{86} values obtained by $RP_{(C18)}$-ESI-$MS_{(qTOF)}$ were examined in three different ways. First, core-TEX_{86} values of $RP_{(C18)}$-ESI-$MS_{(qTOF)}$ were strongly correlated with values of conventional $NP_{(CN)}$-APCI-$MS_{(MSD)}$ (Fig. 5A). The minimal deviation from the 1:1 line likely results from the co-elution of "normal GDGTs" with "shoulder GDGTs" on the RP column (Fig. 4A). The latter compounds are minor lipids and excluded from the TEX_{86} calculation albeit without base-line separation in $NP_{(CN)}$chromatography (Schouten et al., 2007; Becker et al., 2013). However, since the core-

268 TEX_{86} was calibrated for global core-tops using the conventional $NP_{(CN)}$-APCI-MS, we
269 recommend to use normal-phase and APCI to determine TEX_{86} values for palaeoclimate
270 applications. Second, 1G- and 2G-GDGT-TEX_{86} values directly measured by $RP_{(C18)}$-ESI-
271 $MS_{(qTOF)}$ are essentially identical to TEX_{86} values measured by $NP_{(CN)}$-APCI-$MS_{(MSD)}$ after
272 hydrolysis of the isolated 1G- and 2G-GDGT fractions (Fig. 5B). This consistency confirms the
273 fidelity of the new method. Third, the weighted mean IPL-TEX_{86} values directly determined by
274 the $RP_{(C18)}$ method (assuming unity for response factors among individual intact polar GDGTs
275 with different head groups) are similar to the TEX_{86} values obtained by $NP_{(CN)}$-APCI-$MS_{(MSD)}$
276 after hydrolysis of the polar fraction (hydro-TEX_{86}) (Fig. 5C). The observed scatter may result
277 from a combination of varying response factors among different IPL-GDGT classes and/or the
278 release of bound GDGTs from undefined, undetected polar precursors and/or formation of
279 artifacts during hydrolysis.

280 The core- and IPL-specific TEX_{86} values and ring indices obtained by $RP_{(C18)}$-ESI-$MS_{(qTOF)}$
281 show that, for the given sample set (n=11), TEX_{86} values of 1G-GDGTs and 1G-GDGT-PIare
282 lower whereas values of 2G-GDGTs are higher than those of the core GDGTs (Fig. 6A). The
283 ring index generally follows the order 1G-GDGTs $\approx$ core GDGTs > 2G-GDGTs > 1G-GDGT-
284 P1G > 2G-OH-GDGTs $\approx$ 1G-OH-GDGTs (Fig. 6B). These intact polar GDGTs are the
285 biosynthetic products of archaea and will upon head group loss ultimately contribute to the pool
286 of CL-GDGTs (Xie et al., 2013) that is being targeted for GDGT-based proxies. For the intact
287 OH-GDGTs (i.e., 1G-OH-GDGTs and 2G-OH-GDGTs), only cores with 0-2 rings were
288 observed, consistent with previously reported ring distributions of their non-polar derivatives, the
289 core OH-GDGTs (Liu et al., 2012).

290

Version of accepted author manuscript; published in final form in
Organic Geochemistry, 65, 53-62 doi: 10.1016/j.orggeochem.2013.09.012

3.3. Minimizing degradation of labile lipids during ionization and sample preparation

Relative distributions of core ether lipid with varying number of cycloalkyl moieties (e.g., archaeal isoprenoidal GDGTs) and varying degree of methylation (e.g., bacterial branched GDGTs) are well characterized by $NP_{(CN)}$-APCI-MS. However, other structural modifications such as addition of hydroxyl groups (e.g. mono- and di-OH-archaeols) and double bonds (unsaturated archaeols; e.g., Yoshinaga et al., 2011; Yoshinaga et al., 2012) to alkyl chains are also common. The head groups of hydroxylated and unsaturated lipids have been determined using $NP_{(Diol)}$-ESI-MS (e.g., Yoshinaga et al., 2011; Liu et al., 2012), and the detailed structures of core diether derivatives were determined by GC-MS after derivatization (e.g., Nichols and Franzmann, 1992). However, to our knowledge, hydroxylated and unsaturated archaeols determined by the conventional $NP_{(CN)}$-APCI-MS method were not reported. OH-GDGTs, on the other hand, were detected as products of in-source dehydration using a modified $NP_{(CN)}$-APCI-MS method (Liu et al., 2012).

$RP_{(C18)}$-ESI-$MS_{(qTOF)}$ revealed abundant hydroxylated GDGTs and unsaturated and hydroxylated archaeols from a cold seep sediment (sample # 12; Table 1). These lipids were detected as $[M+H]^+$, $[M+NH_4]^+$, and $[M+Na]^+$, with $[M+NH_4]^+$ being the base peak. For comparison, unsaturated and hydroxylated archaeols were not detected using $NP_{(CN)}$-APCI-$MS_{(MSD)}$ for the same sample (Fig. 7A). Moreover, the potential diagnostic fragment ions *m/z* 373.5 or 371.5 that would be obtained upon removal of the OH-group or double bond(s)-bearing phytanyl moiety during MS^2 were not detected either. However, once the interface of $NP_{(CN)}$-APCI-$MS_{(MSD)}$ was replaced by ESI with post-column buffer, i.e., $NP_{(CN)}$-ESI-$MS_{(MSD)}$, unsaturated and hydroxylated archaeols were clearly detected with comparable peak areas to AR (Fig 7B). This suggests that ESI enables superior detection of such labile lipids.

Conventionally employed acid hydrolysis causes additional degradation and by-product formation for these unsaturated and hydroxylated lipids (Sprott et al., 1990; Koga and Morii, 2005; Liu et al., 2012), further reducing their detectability. In contrast, the RP-ESI-MS protocol avoids acid hydrolysis and thus improves the detection of these labile lipids. This advantage is demonstrated by the fact that ratios of [hydrolysis-released OH-GDGTs]/[hydrolysis-released core GDGTs] in polar fractions extracted from a range of sediments (samples # 1-11; Table 1) measured by $NP_{(CN)}$-APCI-$MS_{(MSD)}$ are systematically lower than the ratios of [intact OH-GDGTs]/[intact GDGTs] directly measured by $RP_{(C18)}$-ESI-$MS_{(qTOF)}$ without prior acid hydrolysis (Fig. 8). Enhanced OH-lipid proportion by $RP_{(C18)}$-ESI-$MS_{(qTOF)}$ suggests that they are underestimated by the conventional "hydrolysis + APCI" protocol (e.g., Lipp and Hinrichs, 2009; Liu et al., 2011; Pitcher et al., 2011).

4. Conclusions

We demonstrated the robustness and fidelity of a novel $RP_{(C18)}$-ESI-MS protocol for the analysis of diverse glycerol ether lipid derivatives and related molecular proxies. This method is characterized by 1) high chromatographic resolution for determination of IPL-specific TEX_{86} values and ring indices, 2) greatly improved detection of intact ether lipids (in particular monoglycosyl lipids) as well as core lipids bearing double bonds and hydroxyl groups on their alkyl moieties, and 3) simultaneous characterization of the distribution of core and intact glycerol lipids from crude lipid extracts without further sample preparation, which significantly reduces analytical time and minimizes sample losses. With these advantages, this method offers more accurate and comprehensive glycerol ether lipid fingerprints and opens a new window to study

the mechanisms involved in formation and preservation of glycerol ether lipid-based proxies in the environment.

5. Acknowledgements

We are grateful to the scientists and ship crews of the M84/1 DARCSEAS and SO148/1 cruises and ODP Leg 201 for providing sediment samples from the Mediterranean Sea, the Sea of Marmara, the Black Sea, Hydrate Ridge, and Peru Margin. This work was funded by the Deutsche Forschungsgemeinschaft (DFG) through a postdoctoral fellowship granted through the Cluster of Excellence/Research Center MARUM to C.Z., and through grants Inst 144/300-1 (LC-qTOF system), LI1901/1-1 (J.S.L.), and by the European Research Council under the European Union's Seventh Framework Programme–"Ideas" Specific Programme, ERC grant agreement No. 247153 (to K.-U.H, funding for L.W., K.W.B., J.S.L.).

6. References

Aveldano M.I., Vanrollins M., Horrocks L.A., 1983. Separation and quantitation of free fatty-acids and fatty-acid methyl-esters by reverse phase high-pressure liquid-chromatography. Journal of Lipid Research 24, 83-93.

Becker, K.W., Lipp, J.S., Zhu, C., Liu, X. and Hinrichs, K.-U., 2013. An improved method for the analysis of archaeal and bacterial ether core lipids. Organic Geochemistry 61, 34-44.

Biddle J.F., Lipp J.S., Lever M.A., Lloyd K.G., Sorensen K.B., Anderson R., Fredricks H.F., Elvert M., Kelly T.J., Schrag D.P., Sogin M.L., Brenchley J.E., Teske A., House C.H., Hinrichs K.U., 2006. Heterotrophic Archaea dominate sedimentary subsurface ecosystems off Peru. Proceedings of the National Academy of Sciences of the United States of America 103, 3846-3851.

Bolle M.P., Pardo A., Hinrichs K.U., Adatte T., Von Salis K., Keller G., Muzylev N., 2000.The Paleocene-Eocene transition in the marginal northeastern Tethys (Kazakhstan and Uzbekistan). International Journal of Earth Sciences 89, 390-414.

Byrdwell W.C., 2001. Atmospheric pressure chemical ionization mass spectrometry for analysis of lipids. Lipids 36, 327-346.

Elvert M., Boetius A., Knittel K., Jorgensen B.B., 2003. Characterization of specific membrane fatty acids as chemotaxonomic markers for sulfate-reducing bacteria involved in anaerobic oxidation of methane. Geomicrobiology Journal 20, 403-419.

368 Gibson J.a.E., Miller M.R., Davies N.W., Neill G.P., Nichols D.S., Volkman J.K., 2005.
369 Unsaturated diether lipids in the psychrotrophic archaeon Halorubrum lacusprofundi.
370 Systematic and Applied Microbiology 28, 19-26.
371 Harvey H.R., Fallon R.D., Patton J.S., 1986. The effect of organic-matter and oxygen on the
372 degradation of bacterial-membrane lipids in marine-sediments. Geochimica Et
373 Cosmochimica Acta 50, 795-804.
374 Hinrichs K.U., Hayes J.M., Sylva S.P., Brewer P.G., Delong E.F., 1999. Methane-consuming
375 archaebacteria in marine sediments. Nature 398, 802-805.
376 Hopmans E.C., Schouten S., Pancost R.D., Van Der Meer M.T.J., Sinninghe Damsté J.S., 2000.
377 Analysis of intact tetraether lipids in archaeal cell material and sediments by high
378 performance liquid chromatography/atmospheric pressure chemical ionization mass
379 spectrometry. Rapid Communications in Mass Spectrometry 14, 585-589.
380 Huguet C., Hopmans E.C., Febo-Ayala W., Thompson D.H., Damste J.S.S., Schouten S., 2006.
381 An improved method to determine the absolute abundance of glycerol dibiphytanyl glycerol
382 tetraether lipids. Organic Geochemistry 37, 1036-1041.
383 Huguet C., Martens-Habbena W., Urakawa H., Stahl D.A., Ingalls A.E., 2010. Comparison of
384 extraction methods for quantitative analysis of core and intact polar glycerol dialkyl glycerol
385 tetraethers (GDGTs) in environmental samples. Limnology and Oceanography-Methods 8,
386 127-145.
387 Ikeda M., Kusaka T., 1992. Liquid-chromatography mass-spectrometry of hydroxy and non-
388 hydroxy fatty-Acids as amide derivatives. Journal of Chromatography-Biomedical
389 Applications 575, 197-205.
390 Knappy C.S., Chong J.P.J., Keely B.J., 2009. Rapid discrimination of archaeal tetraether lipid
391 cores by liquid chromatography-tandem mass spectrometry. Journal of the American Society
392 for Mass Spectrometry 20, 51-59.
393 Koga Y., Morii H., 2005. Recent advances in structural research on ether lipids from archaea
394 including comparative and physiological aspects. Bioscience Biotechnology and
395 Biochemistry 69, 2019-2034.
396 Kuypers M.M.M., Blokker P., Erbacher J., Kinkel H., Pancost R.D., Schouten S., Damste J.S.S.,
397 2001. Massive expansion of marine archaea during a mid-Cretaceous oceanic anoxic event.
398 Science 293, 92-94.
399 Larsen A., Mokastet E., Lundanes E., Hvattum E., 2002. Separation and identification of
400 phosphatidylserine molecular species using reversed-phase high-performance liquid
401 chromatography with evaporative light scattering and mass spectrometric detection. Journal
402 of Chromatography B-Analytical Technologies in the Biomedical and Life Sciences 774,
403 115-120.
404 Lipp J.S. and Hinrichs K.U., 2009. Structural diversity and fate of intact polar lipids in marine
405 sediments. Geochimica Et Cosmochimica Acta 73, 6816–6833.
406 Lipp J.S., Morono Y., Inagaki F., Hinrichs K.U., 2008. Significant contribution of Archaea to
407 extant biomass in marine subsurface sediments. Nature 454, 991-994.
408 Liu, X.L., Lipp, J.S., Hinrichs, and K.-U., 2011. Distribution of intact and core GDGTs in marine
409 sediments. Organic Geochemistry, 42, 368-375.
410 Liu X.L., Lipp J.S., Simpson J.H., Lin Y.S., Summons R.E., Hinrichs K.U., 2012. Mono- and
411 dihydroxyl glycerol dibiphytanyl glycerol tetraethers in marine sediments: Identification of
412 both core and intact polar lipid forms. Geochimica Et Cosmochimica Acta 89, 102-115.

Nichols D.S., Davies N.W., 2002. Improved detection of polyunsaturated fatty acids as phenacyl esters using liquid chromatography-ion trap mass spectrometry. Journal of Microbiological Methods 50, 103-113.

Nichols P.D., Franzmann P.D., 1992. Unsaturated diether phospholipids in the antarctic methanogen *Methanococcoides-burtonii*. FEMS Microbiology Letters 98, 205-208.

Oba M., Sakata S., Tsunogai U., 2006. Polar and neutral isopranyl glycerol ether lipids as biomarkers of archaea in near-surface sediments from the Nankai Trough. Organic Geochemistry 37, 1643-1654.

Pearson A., Huang Z., Ingalls A.E., Romanek C.S., Wiegel J., Freeman K.H., Smittenberg R.H., Zhang C.L., 2004. Nonmarine crenarchaeol in Nevada hot springs. Applied and Environmental Microbiology 70, 5229-5237.

Pitcher A., Hopmans E.C., Mosier A.C., Park S.J., Rhee S.K., Francis C.A., Schouten S., Damste J.S.S., 2011. Core and intact polar glycerol dibiphytanyl glycerol tetraether lipids of ammonia-oxidizing archaea enriched from marine and estuarine sediments. Applied and Environmental Microbiology 77, 3468-3477.

Rütters H., Sass H., Cypionka H., Rullkötter J., 2001. Monoalkylether phospholipids in the sulfate-reducing bacteria Desulfosarcina variabilis and *Desulforhabdus amnigenus*. Archives of Microbiology 176, 435-442.

Schouten S., Hopmans E.C., Schefuss E., Sinninghe Damsté J.S., 2002. Distributional variations in marine crenarchaeotal membrane lipids: a new tool for reconstructing ancient sea water temperatures? Earth and Planetary Science Letters 204, 265-274.

Schouten S., Huguet C., Hopmans E.C., Kienhuis M.V.M., Sinninghe Damsté J.S., 2007. Analytical methodology for TEX86 paleothermometry by high-performance liquid chromatography/atmospheric pressure chemical ionization-mass spectrometry. Analytical Chemistry 79, 2940-2944.

Schubotz F., Wakeham S.G., Lipp J.S., Fredricks H.F., Hinrichs K.U., 2009. Detection of microbial biomass by intact polar membrane lipid analysis in the water column and surface sediments of the Black Sea. Environmental Microbiology 11, 2720-2734.

Sommer U., Herscovitz H., Welty F.K., Costello C.E., 2006. LC-MS-based method for the qualitative and quantitative analysis of complex lipid mixtures. Journal of Lipid Research 47, 804-814.

Sprott G.D., Ekiel I., Dicaire C., 1990. Novel, Acid-Labile, Hydroxydiether Lipid Cores in Methanogenic Bacteria. Journal of Biological Chemistry 265, 13735-13740.

Sturt H.F., Summons R.E., Smith K., Elvert M., Hinrichs K.U., 2004. Intact polar membrane lipids in prokaryotes and sediments deciphered by high-performance liquid chromatography/electrospray ionization multistage mass spectrometry - new biomarkers for biogeochemistry and microbial ecology. Rapid Communications in Mass Spectrometry 18, 617-628.

Weijers J.W.H., Schouten S., Van Den Donker J.C., Hopmans E.C., Sinninghe Damsté J.S., 2007. Environmental controls on bacterial tetraether membrane lipid distribution in soils. Geochimica Et Cosmochimica Acta 71, 703-713.

White D.C., Davis W.M., Nickels J.S., King J.D., Bobbie R.J., 1979. Determination of the sedimentary microbial biomass by extractable lipid phosphate. Oecologia 40, 51-62.

Willmann J., Thiele H., Leibfritz D., 2011. Combined Reversed Phase HPLC, Mass spectrometry, and NMR spectroscopy for a fast separation and efficient identification of phosphatidylcholines. Journal of Biomedicine and Biotechnology, doi:10.1155/2011/385786.

Wörmer L.; Lipp J. S.; Schröder J. M.; and Hinrichs K-U. Application of two new LC-ESI-1MS methods for improved detection 2 of intact polar lipids (IPLs) in environmental samples 59, 10–21.

Wuchter C., Schouten S., Coolen M.J.L., Sinninghe Damsté J.S., 2004. Temperature-dependent variation in the distribution of tetraether membrane lipids of marine Crenarchaeota: Implications for TEX_{86} paleothermometry. Paleoceanography 19, doi:10.1029/2004PA001041.

Xie, S., Lipp, J.S., Wegener, G., Ferdelman, T.G., and Hinrichs, K.-U., 2013. Turnover of microbial lipids in the deep biosphere and growth of benthic archaeal populations. Proceedings of the National Academy of Sciences, U.S.A. 110, 6010-6014.

Yoshinaga M.Y., Kellermann M.Y., Rossel P.E., Schubotz F., Lipp J.S., Hinrichs K.U., 2011. Systematic fragmentation patterns of archaeal intact polar lipids by high-performance liquid chromatography/electrospray ionization ion-trap mass spectrometry. Rapid Communications in Mass Spectrometry 25, 3563-3574.

Yoshinaga M.Y., Wörmer L., Elvert M., Hinrichs K.U., 2012. Novel Cardiolipins from Uncultured Methane-Metabolizing Archaea. Archaea-an International Microbiological Journal, doi:10.1155/2012/832097.

Zink K.G., Mangelsdorf K., 2004. Efficient and rapid method for extraction of intact phospholipids from sediments combined with molecular structure elucidation using LC-ESI-MS-MS analysis. Analytical and Bioanalytical Chemistry 380, 798-812.

Version of accepted author manuscript; published in final form in
Organic Geochemistry, 65, 53-62 doi: 10.1016/j.orggeochem.2013.09.012

Figure captions

Fig. 1. Structures of head groups (A) and core (B) ether lipids. PC: phosphocholine; PG: phosphoglycerol; PS: phosphoserine; 1G: monoglycosyl; 2G: diglycosyl; P1G: phospho-monoglycosyl; R= -H or –OH; $GDGT_{0\text{-}5}$: glycerol dialkyl glycerol tetraethers with 0-5 rings, respectively; AR: archaeol. $OH\text{-}GDGT_{0\text{-}2}$: monohydroxylated GDGTs with 0-2 rings, respectively; Note: $GDGT_5$ is crenarchaeol whereas $GDGT_5$' is the regio-isomer of crenarchaeol.

Fig. 2. Intact diethers from TLE aliquots from a cold seep sediment (sample # 12; Table 1) determined by $RP_{(C18)}\text{-}ESI\text{-}MS_{(qTOF)}$ (A) and $NP_{(Diol)}\text{-}ESI\text{-}MS_{(qTOF)}$ (B). Lipids are scanned by $[M+H]^+$, $[M+NH_4]^+$, and $[M+Na]^+$, with peaks of signal to noise ratios (S/N) > 5 being integrated.

Fig. 3. 1G-GDGTs, 2G-GDGTs, and 1G-GDGTs-P1G determined by $RP_{(C18)}\text{-}ESI\text{-}MS_{(qTOF)}$ (A) and $NP_{(CN)}\text{-}ESI\text{-}MS_{(qTOF)}$ (B) in sample # 1 (Table 1). Bar-plots in A denote %individual intact polar GDGTs in a specific group. Lipids are scanned by $[M+H]^+$, $[M+NH_4]^+$, and $[M+Na]^+$, with peaks of S/N > 5 being integrated and filled with colors.

Fig. 4. Chromatographic resolution via $RP_{(C18)}\text{-}ESI\text{-}MS_{(qTOF)}$ of isoprenoidal $GDGT_{0\text{-}5,5'}$ with different number of cycloalkyl moieties (A), branched $GDGT_{I,II,III}$ with different degree of methylation (B), and OH-AR and mono- and di-unsaturated AR (C). Lipid structures and abbreviations refer to Fig. 1. Samples displayed in panels A (# 1), B (# 1), and C (# 12) are listed in Table 1.

505 **Fig. 5.** Plots of TEX_{86} values of core GDGTs (core-TEX_{86}) measured directly by $RP_{(C18)}$-ESI-
506 $MS_{(qTOF)}$ and $NP_{(CN)}$-APCI-$MS_{(MSD)}$ (A); TEX_{86} values of isolated 1G-GDGTs and 2G-GDGTs
507 measured by $RP_{(C18)}$-ESI-$MS_{(qTOF)}$ vs. $NP_{(CN)}$-APCI-$MS_{(MSD)}$ after hydrolysis (B); weight mean
508 IPL-TEX_{86} values directly measured by $RP_{(C18)}$-ESI-$MS_{(qTOF)}$ againstTEX_{86} values derived from
509 hydrolysis-released core GDGTs in the polar fraction (Hydro-TEX_{86}) measured by $NP_{(CN)}$-APCI-
510 $MS_{(MSD)}$(C). The dashed line defines the 1:1 ratio, and samples displayed in panels A and
511 C(sample # 1-11), and in panel B (# 13) are listed in Table 1.

512

513 **Fig. 6.** Core and IPL-specific ring indices (A) and TEX_{86}values (B) determined by $RP_{(C18)}$-ESI-
514 $MS_{(qTOF)}$. Samples (# 1-11) are listed in Table 1.

515

516 **Fig. 7**.Analysis of hydroxylated, mono- and diunsaturated ARs from the same aliquot of a cold
517 seep sediment (# 12; Table 1) using the conventional $NP_{(CN)}$-APCI-$MS_{(MSD)}$ (A) and $NP_{(CN)}$-ESI-
518 $MS_{(MSD)}$ (B) that replaces APCI with ESI but keeps other conditions constant. Lipids are scanned
519 by $[M+H]^+$ and $[M+NH_4]^+$ for $NP_{(CN)}$-APCI-$MS_{(MSD)}$ and $NP_{(CN)}$-ESI-$MS_{(MSD)}$, respectively.

520

521 **Fig. 8.** Comparing the ratios of [hydro-OH-GDGTs]/[hydro-GDGTs] measured by $NP_{(CN)}$-APCI-
522 $MS_{(MSD)}$ to the ratios of [intact-OH-GDGTs]/[intact-GDGTs] measured by $RP_{(C18)}$-ESI-$MS_{(qTOF)}$.
523 The polar fraction was subjected to acid hydrolysis to release core OH-GDGTs (hydro-OH-
524 GDGTs) and core GDGTs (hydro-GDGTs); whereas intact-OH-GDGTs and intact-GDGTs are
525 the sum of all detectable 1G- and 2G-OH-GDGTs for the former group, and 1G-GDGTs, 1G-
526 GDGTs-PI, and 2G-GDGTs for the latter group, respectively, with all IPLs being directly
527 measured by $RP_{(C18)}$-ESI-$MS_{(qTOF)}$ without hydrolysis. The dashed line defines the 1:1 ratio.
528 Numbers denote samples (# 1-11) listed in Table 1.

Version of accepted author manuscript; published in final form in
Organic Geochemistry, 65, 53-62 doi: 10.1016/j.orggeochem.2013.09.012

Figures

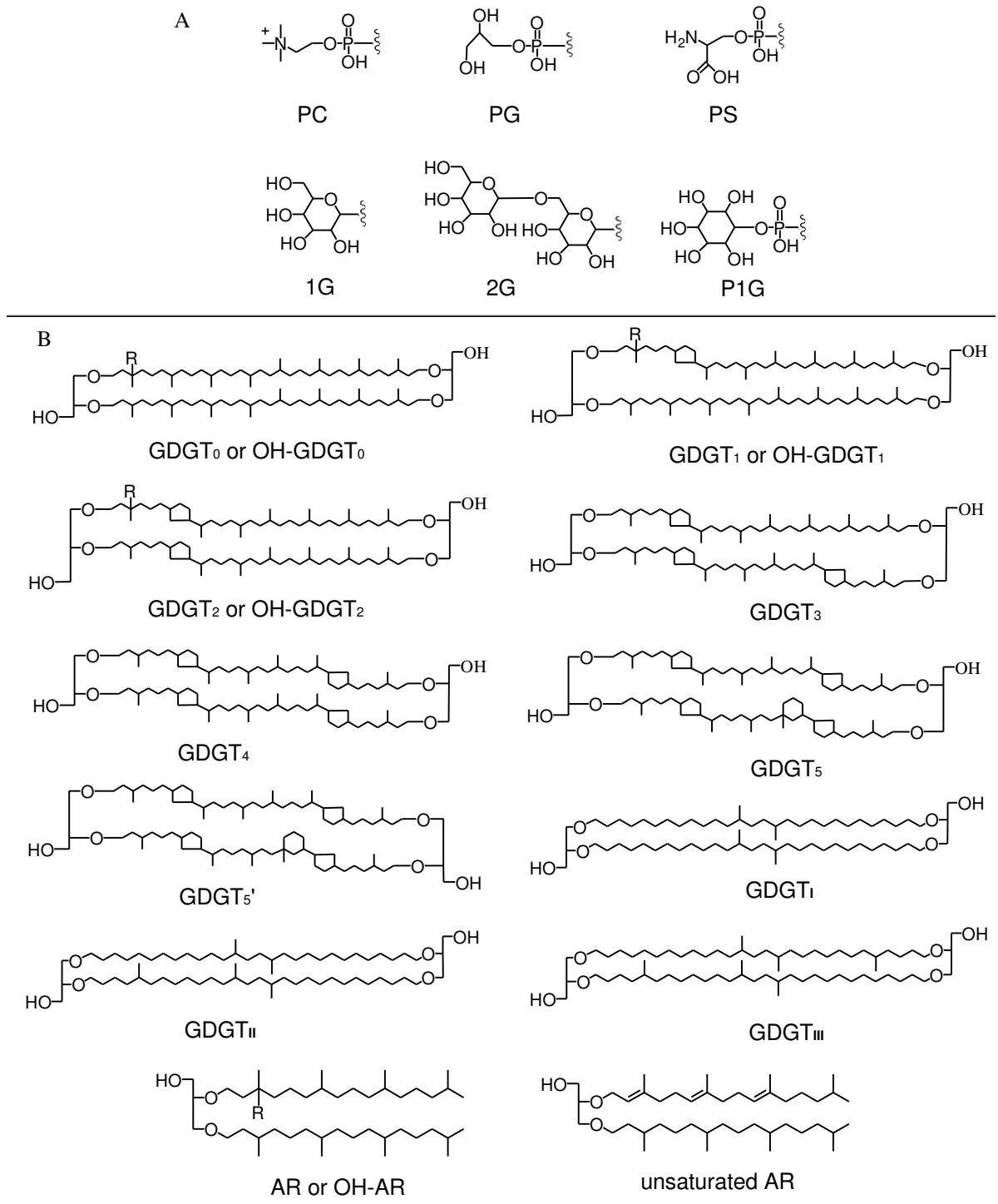

Fig. 1.

Version of accepted author manuscript; published in final form in
Organic Geochemistry, 65, 53-62 doi: 10.1016/j.orggeochem.2013.09.012

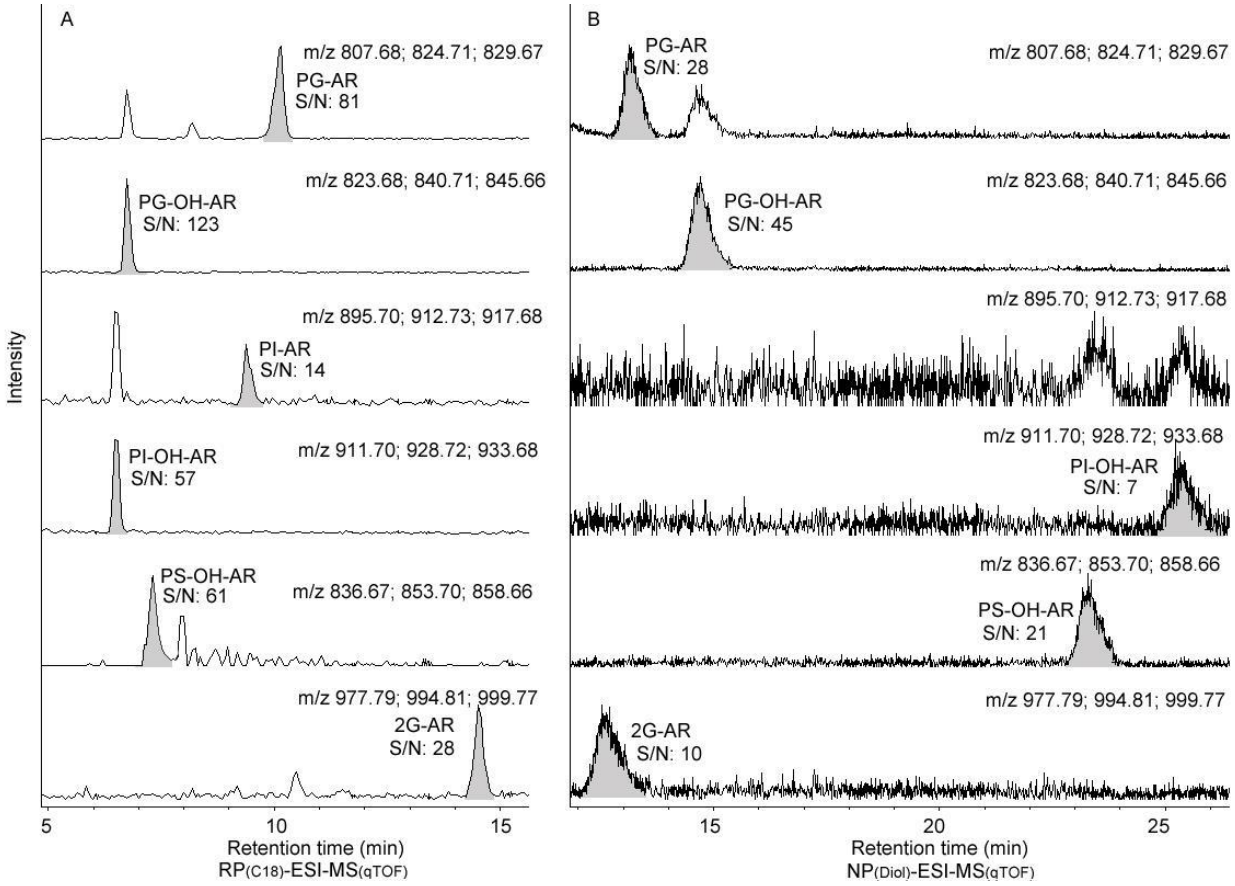

Fig. 2.

Version of accepted author manuscript; published in final form in
Organic Geochemistry, 65, 53-62 doi: 10.1016/j.orggeochem.2013.09.012

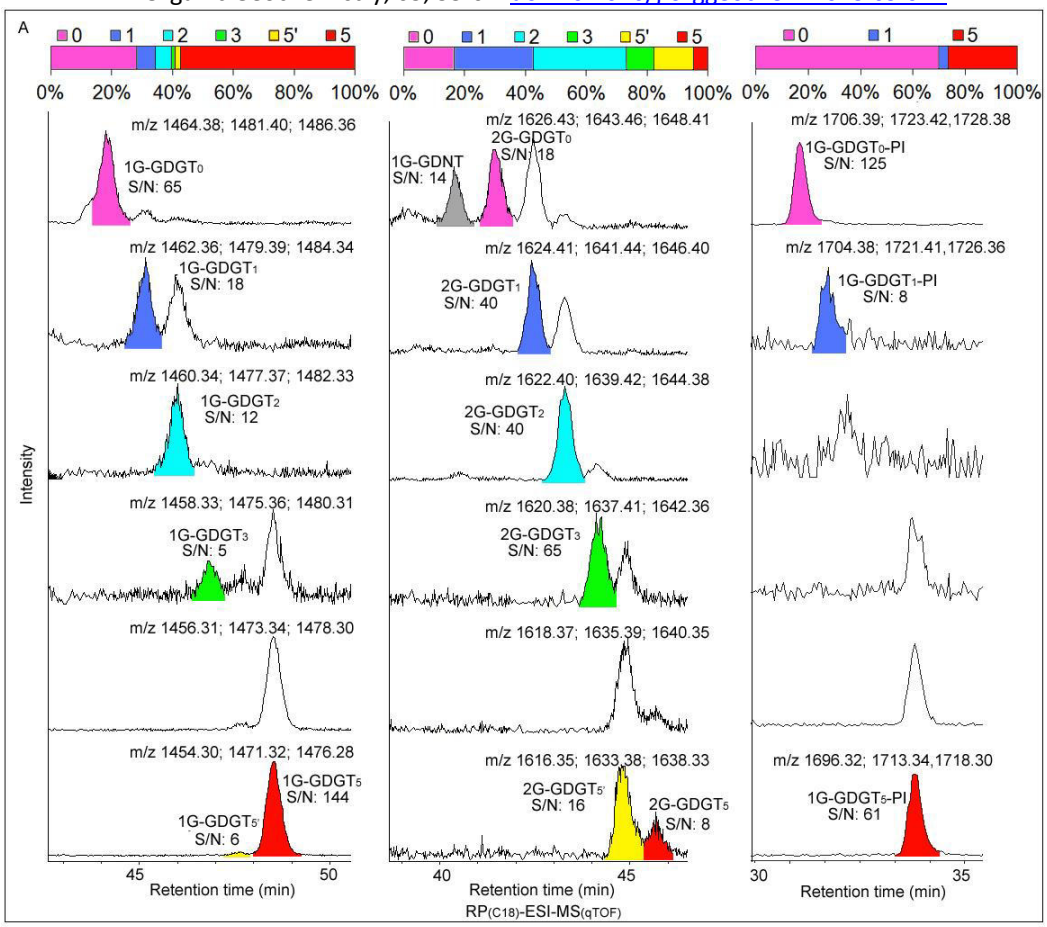

Version of accepted author manuscript; published in final form in
Organic Geochemistry, 65, 53-62 doi: 10.1016/j.orggeochem.2013.09.012

Fig. 3.

Version of accepted author manuscript; published in final form in
Organic Geochemistry, 65, 53-62 doi: 10.1016/j.orggeochem.2013.09.012

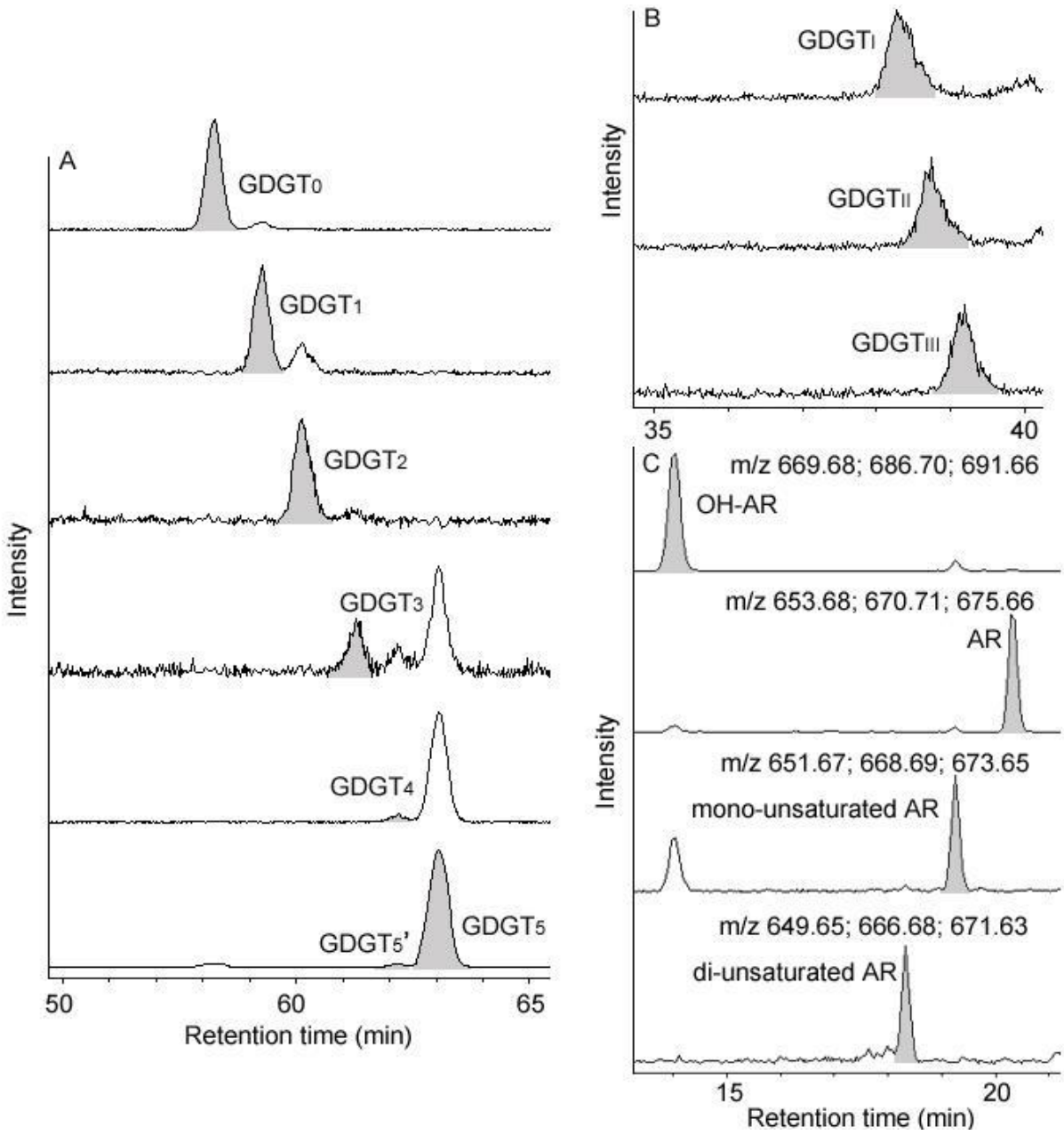

Fig. 4.

Version of accepted author manuscript; published in final form in
Organic Geochemistry, 65, 53-62 doi: 10.1016/j.orggeochem.2013.09.012

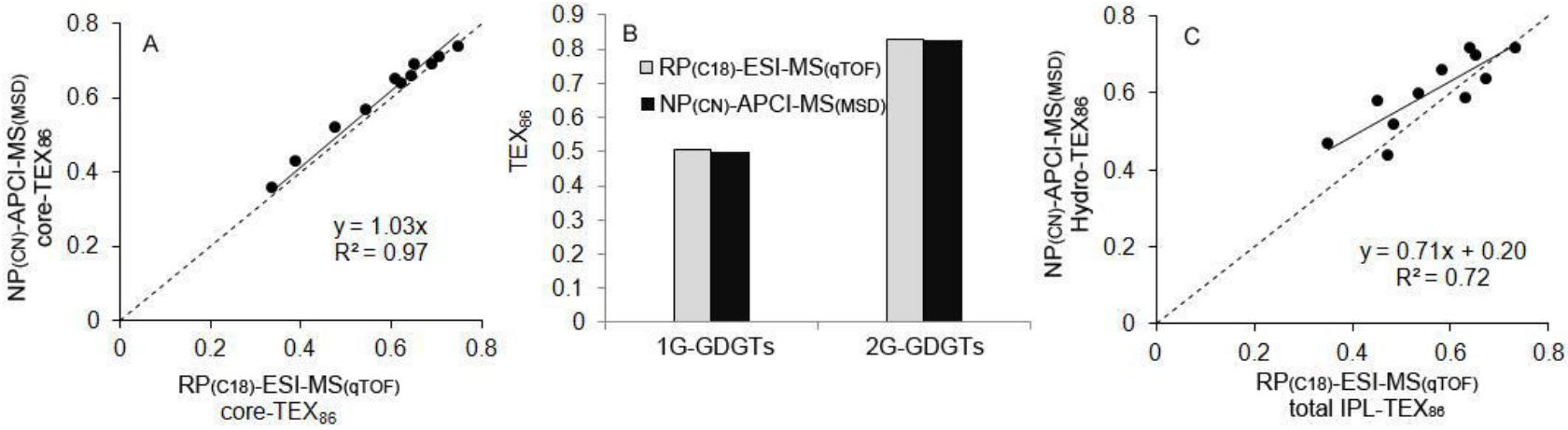

Fig. 5.

Version of accepted author manuscript; published in final form in
Organic Geochemistry, 65, 53-62 doi: 10.1016/j.orggeochem.2013.09.012

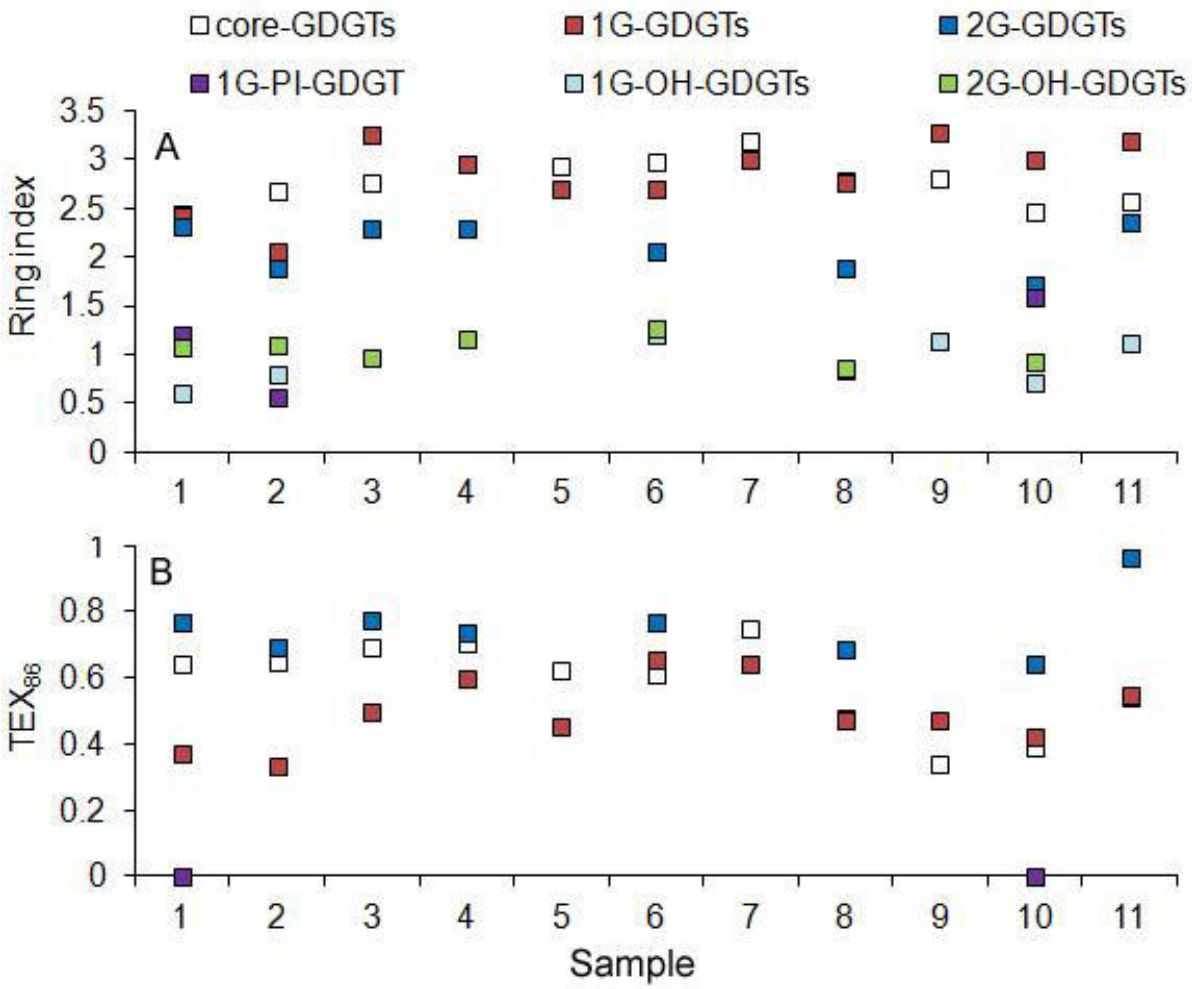

Fig. 6.

Version of accepted author manuscript; published in final form in
Organic Geochemistry, 65, 53-62 doi: 10.1016/j.orggeochem.2013.09.012

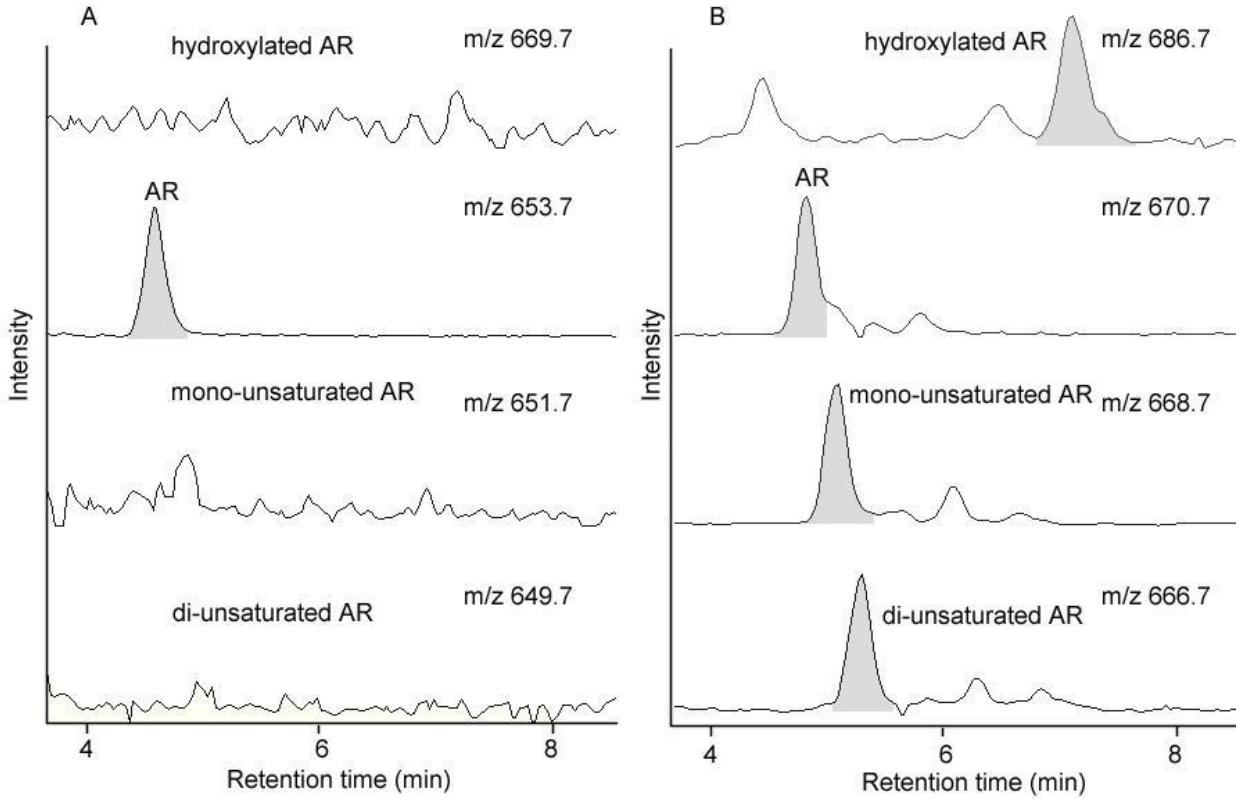

Fig. 7.

Version of accepted author manuscript; published in final form in
Organic Geochemistry, 65, 53-62 doi: 10.1016/j.orggeochem.2013.09.012

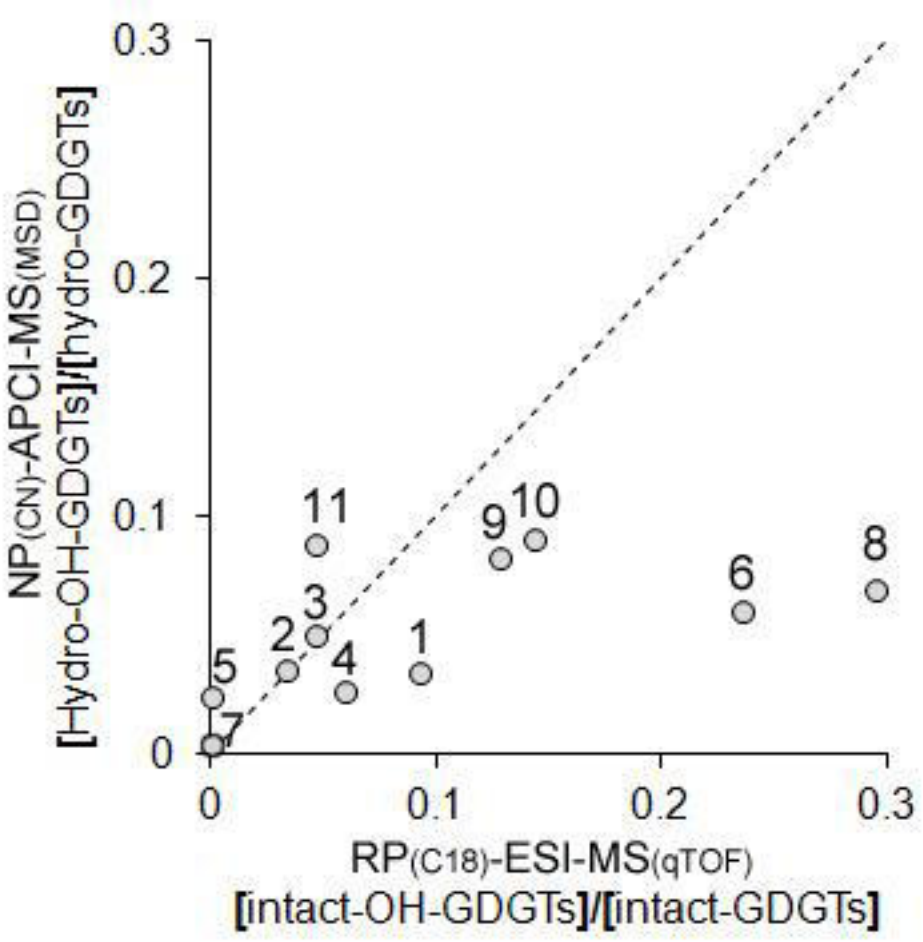

Fig. 8.

Version of accepted author manuscript; published in final form in
Organic Geochemistry, 65, 53-62 doi: 10.1016/j.orggeochem.2013.09.012

Table 1: Samples used in this study

Sample #	Core	Water depth (m)	Interval (cm)	Type	Location	Latitude	Longitude	Cruise
1	GeoB 15102-1	3615	0-2	Marl	Discovery Basin, Mediterranean	35° 16.4' N	21° 41.5' E	
2	GeoB 15102-1		24-34	Marl				
3	GeoB 15102-5		177-191	Marl				
4	GeoB 15103-2	1367	21-34	Sapropel	Eastern Mediterranean	33° 2.0' N	32° 38.0' E	M84/1
5	GeoB 15103-2		220-240	Marl				
6	GeoB 15103-2		435-455	Sapropel				
7	GeoB 15103-2		10-12	Marl				
8	GeoB 15104-2	600	283-296	Sapropel	Sea of Marmara	40° 48.0' N	27° 43,5' E	
9	GeoB 15104-2		620-635	Marl				
10	GeoB 15105-2	1266	147-162	Marl	Black Sea	41° 31.7' N	30° 53,1' E	
11	GeoB 15105-2		420-435	Marl				
12	GeoB12320	550	8-10	Cold seep	Off Pakistan	24°53'N	63°01'E	M74/3
13	ODP 1227A-2H2	427	845-860	Mud	Peru Margin	2° 46.2' N	110° 34.3' W	ODP Leg 201

Version of accepted author manuscript; published in final form in
Organic Geochemistry, 65, 53-62 doi: 10.1016/j.orggeochem.2013.09.012

Table 2: Chromatographic details of LC-MS analysis for glycerol ether lipids.

Protocol	RP_{C18}-ESI-MS_{qTOF}	NP_{Diol}-ESI-MS_{qTOF}	NP_{CN}-APCI-MS_{MSD}
		Chromatography	
Column	ACE3 C_{18}	LiChrospher Diol	Prevail Cyano
Dimension	150 × 2.1 mm	150 × 2.1 mm	150 × 2.1 mm
Particle size	3µm	5µm	3µm
Eluent A	methanol/formic acid/14.8 M NH_3aq (100/0.04/0.10)	*n*-hexane/2-propanol/formic acid/14.8 M NH_3aq (79/20/0.12/0.04)	*n*-hexane/2-propanol (99:1)
Eluent B	2-propanol/formic acid/14.8 M NH_3aq (100/0.04/0.10)	2-propanol/water/formic acid/14.8 M NH_3aq (88/10/0.12/0.04)	*n*-hexane: 2-propanol (90:10)
Gradients	100% A for 10 min → a rapid gradient to 24% B over 5 min → a slow gradient to 65% B over another 55 min → cleaning (90% B) and re-equilibrating (100% A)	a gradient of 100% A to 35% A and 65% B in 45 min → hold for 20 min → cleaning (100% B) and re-equilibrating (100% A)	100% A for 5 min →a gradient to 9% B over 45 min → cleaning (100% B) and re-equilibrating (100% A)
flow rate (mL/min)	0.2	0.2	0.2
Column temp.	45°C	30°C	30°C
Sample solvent	methanol	methanol/dichloromethane (1:5, v/v)	*n*-hexane: 2-propanol (99:1)
Ref.	This study	Sturt et al., 2004	Schouten et al., 2007